

# Minimal Adversarial Examples for Deep Learning on 3D Point Clouds

Jaeyeon Kim<sup>1</sup>    Binh-Son Hua<sup>2,3</sup>    Duc Thanh Nguyen<sup>4</sup>    Sai-Kit Yeung<sup>1</sup>

<sup>1</sup>Hong Kong University of Science and Technology

<sup>2</sup>VinAI Research, Vietnam

<sup>4</sup>Deakin University

<sup>3</sup>VinUniversity, Vietnam

## Abstract

*With the recent developments of convolutional neural networks, deep learning for 3D point clouds has shown significant progress in various 3D scene understanding tasks including 3D object recognition. In a safety-critical environment, it is however not well understood how such neural networks are vulnerable to adversarial examples. In this work, we explore adversarial attacks for point cloud-based neural networks with a focus on real-world data. We propose a general formulation for adversarial point cloud generation via  $\ell_0$ -norm optimisation. Our method generates adversarial examples by attacking the classification ability of the point cloud-based networks while considering the perceptibility of the examples and ensuring the minimum level of point manipulations. The proposed method is general and can be realised in different attack strategies. Experimental results show that our method achieves the state-of-the-art performance with 80% of attack success rate while manipulating only about 4% of the points. We also found that compared with synthetic data, real-world point cloud classification is more vulnerable to attacks.*

## 1. Introduction

Deep learning has shown great potentials in solving a wide spectrum of computer vision tasks. In life-crucial applications, one concern is that deep neural networks can be vulnerable to adversarial examples, a special kind of inputs that can fool the networks to make undesirable predictions. Several adversarial attack techniques have been proposed to generate such examples. By contrast, adversarial defense methods have been developed to detect and neutralise adversarial examples. Therefore, understanding how adversarial attacks and defenses operate is of great importance to make deep learning techniques more reliable and robust.

With the growing popularity of low-cost 3D sensors and light-field cameras, the community has also started investigating the vulnerability of neural networks on 3D data, especially 3D point clouds [30, 13, 12, 31, 27]. However, existing works focus on common scenarios, such as gener-

ating adversarial point clouds by perturbing points in input point clouds. While such approaches have a high attack success rate, the perturbations are not imperceptible and can be easily defended by outlier detection or noise removal algorithms. In addition, existing adversarial attack methods do not perform optimally since all points in point clouds are involved in the manipulation.

In this work, we investigate 3D adversarial attacks and defenses in more extreme but practical settings. First, we explore how to generate adversarial point clouds such that the number of points perturbed from the original point cloud is minimal while maintaining the perceptibility of the point cloud. We propose a new formulation for adversarial point cloud generation that can be adapted to various settings and realised in different attack strategies. Second, we explore adversarial attacks to point clouds obtained from real-world 3D scans. We show that networks trained with real-world 3D point clouds are more vulnerable to attacks than networks trained with synthetic data. In summary, our contributions include:

- A new technique to generate minimal adversarial point clouds. We formulate the problem using an  $\ell_0$  optimisation that can then be approximately solved by an  $\ell_1$  optimisation;
- A new theoretical formulation that generalises two adversarial point clouds generation techniques: point perturbation and point addition;
- A benchmark on adversarial attacks on both synthetic and real-world 3D point clouds.

## 2. Related Work

In this section, we review 3D deep learning techniques, especially those working on 3D point clouds. We then discuss adversarial attack and defense methods in 3D in general and some variants that assume similar extreme settings to that we use in this paper.

**3D Deep Learning.** Recent availability of 3D datasets [29, 3, 7, 1, 5, 2, 25] has led to significant

advances in deep learning on 3D data. In this domain, several works focus on designing convolution operations to make convolutional neural networks learn features from point clouds directly [19, 20, 11, 8, 26, 23, 9, 35]. Some convolutions are extended to support rotation invariance [21, 34, 18, 32]. Such convolutions allow scene understanding tasks such as object recognition, semantic segmentation, and object detection to be trained directly with 3D point clouds, achieving competitive performance.

In this work, we use PointNet [19] as the base neural network to investigate adversarial examples. Among the mentioned 3D datasets, we use ModelNet40 [29] and ScanObjectNN [25] for our experiments. ModelNet40 contains a collection of CAD models used for benchmarking state-of-the-art object classification techniques. ScanObjectNN is a dataset of real-world 3D point clouds designed to further benchmark the performance of object classification.

**Adversarial Point Clouds.** There exist a few studies on adversarial attacks and defenses for point cloud classification [30, 13, 12, 31, 27]. For instance, Xiang et al. [30] first suggested an optimisation algorithm based on C&W framework [16] using the Chamfer and Hausdorff distance. Liu et al. [13] extended the fast gradient sign method (FGSM) in [6] to 3D point clouds and showed how to construct adversarial examples using mesh and clipping norm. In general, the basic ideas in these works follow previous adversarial attack techniques in 2D domain, which focus on how a point cloud should be perturbed to make an adversarial example. Readers are referred to [33] for a comprehensive review on adversarial attacks and defenses on images.

Several works suggest viable perturbation techniques on point clouds. For instance, adversarial point clouds can be generated by perturbing points individually [30] or in bundles [30, 12, 31]. It is also possible to mix newly added points with perturbed points in a point cloud to make an adversarial example [12]. Alternatively, some methods opt to drop points based on point saliency [36, 28]. There are also works [12, 27] that further consider perceptibility constraints applied to local meshes.

In contrast to adversarial attacks, countermeasures for adversarial point clouds have been so far scarce. Typical approaches to defense include removing outliers or salient points [13] and noise removal [37, 31]. In the latter case, the authors proposed to use a neural network that consists of a new layer for outlier removal combined with point cloud upsampling.

**Minimal Adversarial Attacks.** In 2D domain, there is a specific family of techniques that focus on perturbing a minimum number of pixels in adversarial attacks. For instance, Papernot et al. [17] perturbed pixels by considering the saliency map based on gradients. Carlini et al. [16] ex-

tended this method and used  $\ell_0$  optimisation to minimise the number of pixels to perturb. Recently, Modas et al. [14] and Croce et al. [4] focused on how to perturb a sparse set of pixels but still achieved good perceptibility. Local search and evolutionary algorithms are also applied to obtain sparse perturbations [15, 24, 22]. In this paper, we also explore adversarial attacks that only perturb a minimal set of points. However, unlike the above works, we propose a new formulation that is able to generalise various adversarial point cloud generation strategies.

### 3. Proposed Method

We propose a general formulation for adversarial attacks to 3D point clouds using  $\ell_0$  optimisation. We show that our formulation can be adapted to various settings and realised in different attack strategies.

Our problem of interest can be stated as follows. Let  $P = \{\mathbf{p}_1, \dots, \mathbf{p}_N\}$  be an input set of  $N$  points where each point  $\mathbf{p}_i$  is represented by a vector of its coordinates  $\mathbf{p}_i = [p_{i,x}, p_{i,y}, p_{i,z}]^\top \in \mathbb{R}^3$ . Let  $F$  denote a point-based neural network, e.g., PointNet [19], and  $F_i(P)$  denote the probability that the point set  $P$  is classified into the  $i$ -th class or the  $i$ -th element of the logits of the input of softmax layer. If  $i^*$  is the true class label of the point cloud  $P$ , then  $i^* = \operatorname{argmax}_i F_i(P)$ . Let  $P'$  be an adversarial example of  $P$ . We aim to find  $P'$  such that  $\operatorname{argmax}_i F_i(P) \neq \operatorname{argmax}_i F_i(P')$ , i.e.,  $P'$  and  $P$  are classified into different classes by the network  $F$ .

In the following, we present a general model to generate  $P'$  using  $\ell_0$  optimisation and describe in details two different ways to realise our model: point perturbation and point addition.

#### 3.1. Point Perturbation

##### 3.1.1 Formulation

Given a point cloud  $P$ , we aim to find a minimal set of points that can be shifted to generate an adversarial point cloud  $P'$  to attack the network  $F$ . In this case, the adversarial point cloud  $P'$  generated by the point perturbation process will have the same number of points (with  $P$ ). Intuitively, the point perturbation process must satisfy the following conditions: (i) the perceptibility of the point cloud is maintained during the perturbation, i.e., the perturbed point cloud  $P'$  should not much deform from the original point cloud  $P$ ; (ii) a minimal number of points in  $P$  are selected for perturbation; and (iii) the original point cloud  $P$  and perturbed point cloud  $P'$  are classified into different classes by the network  $F$ .

We express the selection of points in  $P$  for perturbation by a binary indication vector  $\mathbf{a} = [a_1, \dots, a_N]^\top \in \{0, 1\}^N$  where  $a_i$  is 1 if  $\mathbf{p}_i$  is selected, and 0 otherwise. Suppose that  $E = \{\mathbf{e}_1, \dots, \mathbf{e}_N\}$  is the set of perturbations, in which

$\mathbf{e}_i = [e_{i,x}, e_{i,y}, e_{i,z}]^\top \in \mathbb{R}^3$  is the perturbation vector to be applied on  $\mathbf{p}_i$  to obtain  $\mathbf{p}'_i$ . Applying perturbation set  $E$  on the point cloud  $P$  results in an adversarial point cloud  $P'$  as

$$P' = \{\mathbf{p}'_i = \mathbf{p}_i + a_i \mathbf{e}_i \mid \mathbf{p}_i \in P\}. \quad (1)$$

The process of generation of  $P'$  can be formulated as,

$$\begin{aligned} \min_{\mathbf{a}, E} f(P, \mathbf{a}, E) &= \min_{\mathbf{a}, E} \{\lambda_1 \|\mathbf{a}\|_0 + \lambda_2 D(P, P')\} \\ \text{s.t.} \quad \arg\max_i F_i(P) &\neq \arg\max_{i'} F_{i'}(P') \end{aligned} \quad (2)$$

where  $\|\mathbf{a}\|_0 = \#\{i : a_i \neq 0, i = 1, \dots, N\}$  is the  $\ell_0$  norm of  $\mathbf{a}$  (i.e., the number of non-zero elements in  $\mathbf{a}$ ) and  $D(P, P')$  is some distance between  $P$  and  $P'$ .

The optimisation problem defined in Equation (2) covers all the aforementioned conditions. In particular, the first term,  $\|\mathbf{a}\|_0$  in the objective function  $f(P, \mathbf{a}, E)$  imposes the quantity of selected points in the point selection process while the second term,  $D(P, P')$  constrains the perceptibility of the adversarial point cloud  $P'$  w.r.t. the original point cloud  $P$ . As will be explained later in this section,  $D(P, P')$  can be defined using different distance metrics. The constraint  $\arg\max_i F_i(P) \neq \arg\max_{i'} F_{i'}(P')$  ensures the generated point cloud  $P'$  can fool the network  $F$ , i.e.,  $F$  would not classify  $P$  and  $P'$  into the same class.

However, the search space of (2) is too large, e.g.,  $\mathcal{O}(2^N - 1)$  for a set of  $N$  points. In order to reduce the search space, salient map [36] and critical points [19] can be used. Qi et al. [18] suggested the concept of critical points which are a subset of the input point cloud that has a great impact on the classification output. Furthermore, critical points can be ranked by their distances from the nearest points in the point cloud [28]. In this work, we use saliency map and critical points to initialize our solution when optimizing Equation (2).

### 3.1.2 Relaxed Formulation

To solve the constrained optimisation problem in (2), we convert it into an unconstrained optimisation problem using a Lagrange multiplier-like form as:

$$\begin{aligned} \min_{\mathbf{a}, E} f(P, \mathbf{a}, E) \\ = \min_{\mathbf{a}, E} \{\lambda_1 \|\mathbf{a}\|_0 + \lambda_2 D(P, P') + \lambda_3 h(P')\} \end{aligned} \quad (3)$$

where, like [30], we define,

$$h(P') = \max \left\{ 0, F_{i^*}(P') - \max_{i' \neq i^*} F_{i'}(P') \right\} \quad (4)$$

where  $i^*$  is the true class label of the point set  $P$ .

The problem in (3) is NP-hard in general and thus can be relaxed as

$$\begin{aligned} \min_{\mathbf{a}, E} f(P, \mathbf{a}, E) \\ = \min_{\mathbf{a}, E} \{\lambda_1 \|\mathbf{a}\|_1 + \lambda_2 D(P, P') + \lambda_3 h(P')\} \end{aligned} \quad (5)$$

where  $\|\mathbf{a}\|_1 = \sum_{i=1}^N a_i$  is the  $\ell_1$  norm of  $\mathbf{a}$ .

The optimisation problem defined in (10) formulates our proposed adversarial generation method. This formulation is general and can be adapted conveniently to other adversarial generation strategies, e.g., point addition.

### 3.1.3 Perceptibility

There are several ways to realise the perceptibility  $D(P, P')$  in (10). If we assume the correspondence between each point  $\mathbf{p}_i \in P$  and its perturbed point  $\mathbf{p}'_i \in P'$  defined in (11) is maintained, then we can define  $D(P, P')$  using Euclidean distances between  $\mathbf{p}_i$  and  $\mathbf{p}'_i$  as

$$D_{Euclidean}(P, P') = \frac{1}{N} \sum_{i=1}^N (a_i \|\mathbf{e}_i\|_2). \quad (6)$$

However, such correspondences are not always well defined, e.g., when the number of points changes in the case of point addition, making Euclidean distance not a valid choice. We further propose to use Chamfer distance and Hausdorff distance to measure perceptibility. Specifically, we can define  $D(P, P')$  as

$$\begin{aligned} D_{Chamfer}(P, P') &= \max \left\{ \frac{1}{|P|} \sum_{\mathbf{p}_i \in P} \min_{\mathbf{p}'_j \in P'} \|\mathbf{p}_i - \mathbf{p}'_j\|_2, \right. \\ &\quad \left. \frac{1}{|P'|} \sum_{\mathbf{p}'_j \in P'} \min_{\mathbf{p}_i \in P} \|\mathbf{p}'_j - \mathbf{p}_i\|_2 \right\} \end{aligned} \quad (7)$$

or

$$\begin{aligned} D_{Hausdorff}(P, P') &= \max \left\{ \max_{\mathbf{p}_i \in P} \left\{ \min_{\mathbf{p}'_j \in P'} \|\mathbf{p}_i - \mathbf{p}'_j\|_2 \right\}, \right. \\ &\quad \left. \max_{\mathbf{p}'_j \in P'} \left\{ \min_{\mathbf{p}_i \in P} \|\mathbf{p}'_j - \mathbf{p}_i\|_2 \right\} \right\}. \end{aligned} \quad (8)$$

Note that, as defined in (7) and (8), the Chamfer distance and Hausdorff distance do not require the same of number of points in both the point clouds  $P$  and  $P'$ . Hence, they can be adapted easily to different point generation methods, e.g., point addition, presented in subsequent sections.

Since the optimisation problem in (10) is a 0/1 integer program, we further relax it by finding a continuous solution  $\hat{\mathbf{a}} = [\hat{a}_1, \dots, \hat{a}_N]^\top$  where  $\hat{a}_i \in [0, 1]$ . Iterative gradient methods [6, 13], can be applied to solve (10). In our implementation, we initialised  $\hat{\mathbf{a}}$  by setting  $\hat{a}_i = 1$  if  $\mathbf{p}_i$  is a

critical point and  $\hat{a}_i = 0$ , otherwise. We applied the method in [19] to find the critical points. We empirically observe that this initialisation scheme improved attack success rate. Finally, we achieve the final solution  $\mathbf{a}$  as,

$$a_i = \begin{cases} 0, & \text{if } \hat{a}_i \leq 0.5 \\ 1, & \text{otherwise.} \end{cases} \quad (9)$$

It is worth noting that in practice, for point perturbation, the exact value of  $a_i$  is not important as our goal is to generate the adversarial examples. We can skip the thresholding and simply use the approximation  $\hat{a}_i \mathbf{e}_i$  as the offset to obtain the adversarial point cloud.

### 3.2. Point addition

In addition to point perturbation, we can generate an adversarial example  $P'$  by extending  $P$  with a minimum number of additional points. We show that our proposed formulation in (10) can also be applied in this task. Specifically, suppose that there are no more than  $K$  points added to the original point cloud  $P$ . We can construct a new point set  $\tilde{P}$  including all the points in  $P$  and  $K$  new points. These  $K$  new points can be generated by randomly choosing  $K$  points in  $P$  and adding them to  $\tilde{P}$ . Alternatively, one may choose these  $K$  points from the critical point set [19]. We note that this way of construction of  $\tilde{P}$  does not change the perceptibility of  $P$  as  $D(P, \tilde{P}) = 0$  for either the Chamfer or Hausdorff distance used to define  $D(P, \tilde{P})$ . In addition, both  $P$  and  $\tilde{P}$  are treated equally by the network  $F$ , i.e.,  $\forall i, F_i(P) = F_i(\tilde{P})$ , as the geometric structure of the point clouds remains unchanged.

Similarly, we also construct a vector  $\tilde{\mathbf{a}} = [\tilde{a}_1, \dots, \tilde{a}_{N+K}]^T \in \{0, 1\}^{N+K}$  and a perturbation set  $\tilde{E} = \{\tilde{\mathbf{e}}_1, \dots, \tilde{\mathbf{e}}_{N+K}\}$  by extending  $\mathbf{a}$  and  $E$  with  $K$  new elements and solve the optimisation problem in (10) with a new objective function  $f(\tilde{P}, \tilde{\mathbf{a}}, \tilde{E})$ . The vector  $\tilde{\mathbf{a}}$  is initialised as follows,  $\tilde{a}_i$  is set to 1 for  $i \in \{1, \dots, N\}$ , and to a random value in  $\{0, 1\}$ , otherwise. Furthermore, during the optimisation process, we fix  $\tilde{a}_i = 1, \forall i = 1, \dots, N$ , i.e., original points in  $P$  will not be changed. Finally, the adversarial point cloud  $P'$  is obtained by including points  $\tilde{\mathbf{p}}_i \in \tilde{P}$  such that  $\tilde{a}_i = 1$ .

## 4. Experiments

### 4.1. Experiment Setup

**Datasets.** We used ModelNet40 [29] and ScanObjectNN [25] datasets to evaluate our proposed method. The ModelNet40 dataset is a popular benchmark for classification of 3D CAD models. It consists of 40 object categories, 9,843 models for training and 2,468 models for testing. We followed Qi et al. [19] to sample the surfaces of the 3D models uniformly and then normalise the points into a unit cube.

The ScanObjectNN dataset is an object dataset from real-world indoor scans. It is designed to evaluate object classification in more practical settings that involve view occlusions and object partiality. ScanObjectNN has 15 object categories and five challenging variants including objects with background, translated objects, rotated objects, and scaled objects. We also followed Uy et al. [25] to normalise the point clouds using mean and furthest point distance with data containing background.

**Implementation Details.** We adopted PointNet [19] as the targeted network which was used for generating adversarial examples and for attacks. We trained PointNet with the same settings used in the original paper. For point clouds with varying sizes, we modified the max-pooling operator in the network accordingly [36]. For our method, we used Adam optimiser with learning rate of 0.01. We performed an exhaustive search for the parameters in (10) and empirically set them as  $\lambda_1 = 1, \lambda_2 = 550, \lambda_3 = 9$ . And  $\lambda_1 = 1, \lambda_2 = 1500, \lambda_3 = 9$  for PointNet++. We run 250 iterations of stochastic gradient descents in our optimization. To make the optimisation more efficient, we initialised the vector  $\mathbf{a}$  in (10) using critical points, i.e.,  $a_i = 1$  if  $\mathbf{p}_i$  is a critical point. The experiments for different initialization are in the supplementary.

### 4.2. Evaluation

#### 4.2.1 Baselines

As there is very few work that focuses on the minimality of adversarial point clouds, we adopted existing adversarial attack methods [36, 28] to make the baselines. Specifically, we make our baselines by using techniques proposed by Xiang et al. [30] that can only move a fixed number of points, and by Zheng et al. [36] and Wicker et al. [28] that removes a small set of points based on their importance. Our baselines include: (a) random point selection, i.e., randomly selecting points for perturbation and addition, (b) saliency-based point selection [36] using (b.1) critical count, (b.2) low-score points, (b.3) high-score points, and (c) critical neighbors [28]. For baseline (a), we randomly sample points in an input point cloud uniformly. For (b.1), we use the critical count algorithm in [36] that considers the number of max-pooled features to rank critical points. For (b.2) and (b.3), we first compute a point cloud saliency map for the input point cloud and choose the points based on the saliency scores. Low- and high-score points refer to two opposite ranking strategies that choose the lowest or highest impact points. For (c), we implement the critical neighbor method [28] that selects critical points based on their distances from nearby points.



	Success Rate	Chamfer Distance	Hausdorff Distance	# Points
(a) Random	55.56	$7.47 \times 10^{-4}$	$2.49 \times 10^{-3}$	413
(b.1) Critical count [36]	56.52	$7.35 \times 10^{-4}$	$2.49 \times 10^{-3}$	406
(b.2) Low-score [36]	55.97	$6.47 \times 10^{-4}$	$2.50 \times 10^{-3}$	358
(b.3) High-score [36]	58.39	$7.52 \times 10^{-4}$	$2.48 \times 10^{-3}$	424
(c) Critical neighbor [28]	27.75	$1.86 \times 10^{-4}$	$3.67 \times 10^{-2}$	50
Ours	<b>86.51</b>	<b><math>1.40 \times 10^{-4}</math></b>	$1.67 \times 10^{-2}$	<b>34</b>

(a) Point Perturbation

	Success Rate	Chamfer Distance	Hausdorff Distance	# Points
(a) Random	43.90	$2.16 \times 10^{-4}$	$2.49 \times 10^{-3}$	121
(b.1) Critical count [36]	45.13	$2.13 \times 10^{-4}$	$2.49 \times 10^{-3}$	118
(b.2) Low-score [36]	60.96	$1.64 \times 10^{-4}$	$2.50 \times 10^{-3}$	89
(b.3) High-score [36]	41.06	$2.27 \times 10^{-4}$	$2.49 \times 10^{-3}$	128
(c) Critical neighbor [28]	11.16	$1.26 \times 10^{-4}$	$2.50 \times 10^{-3}$	66
Ours	<b>84.00</b>	$1.36 \times 10^{-4}$	$1.83 \times 10^{-2}$	<b>31</b>

(b) Point Addition

Table 1. Attack performance to PointNet on ModelNet40.

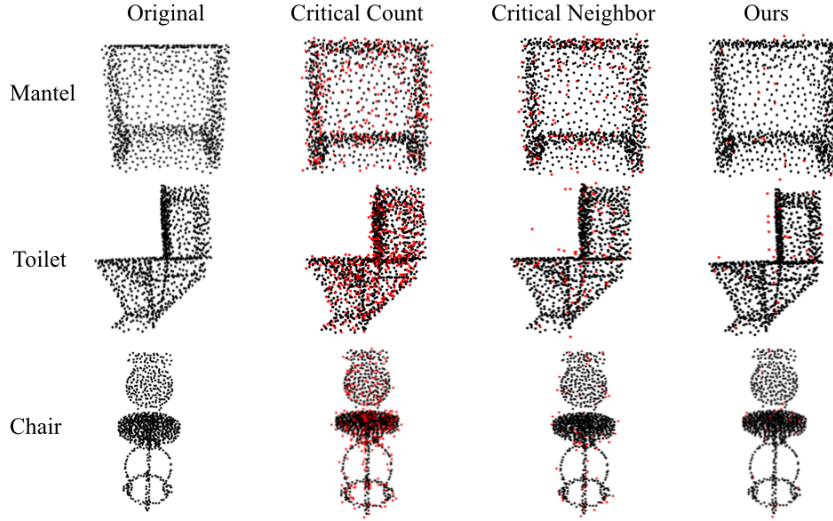


Figure 1. Adversarial examples generated by our method from ModelNet40. Red points represent selected points.

#### 4.2.2 Attack Results

We report the attack success rate, the perceptibility, and the number of points used in each baseline and our method in Table 1 (on ModelNet40) and Table 2 (on ScanObjectNN) respectively. The number of points are reported as the rounded average of all perturbed points. We evaluate the perceptibility using Chamfer and Hausdorff distance. We note that ScanObjectNN has five different variants. In this experiment, we used “OBJ\_BG”, the variant adding background to objects.

In general, on ModelNet40, our method achieves good

success rate while requiring a small number of processing points compared with other methods. In particular, our method only uses 3% of the total input points to reach 86% of success rate. Except the critical neighbor [28], other baseline methods require roughly  $10\times$  larger point sets than our method does while achieving much lower success rate. Compared with the critical neighbor [28], our method uses similar number of points but our success rate is more than  $2\times$  higher. Similar performance is found on the OBJ\_BG variant of ScanObjectNN dataset (see Table 2). The generated adversarial examples are also highly imperceptible; this is shown quantitatively by the small values of both the

	Success Rate	Chamfer Distance	Hausdorff Distance	# Points
Random	63.72	$6.10 \times 10^{-4}$	$2.50 \times 10^{-3}$	340
Critical Count [36]	64.97	$6.09 \times 10^{-4}$	$2.50 \times 10^{-3}$	340
Low-Drop [36]	63.81	$5.49 \times 10^{-4}$	$2.50 \times 10^{-3}$	306
High-Drop [36]	66.82	$6.16 \times 10^{-4}$	$2.47 \times 10^{-3}$	350
Critical Neighbor [28]	38.48	$1.72 \times 10^{-4}$	$3.83 \times 10^{-2}$	35
Ours	<b>84.37</b>	<b><math>9.83 \times 10^{-5}</math></b>	$1.01 \times 10^{-2}$	<b>28</b>

(a) Point Perturbation

	Success Rate	Chamfer Distance	Hausdorff Distance	# Points
Random	60.05	$1.77 \times 10^{-4}$	$2.50 \times 10^{-3}$	97
Critical Count [36]	59.63	$1.79 \times 10^{-4}$	$2.49 \times 10^{-3}$	97
Low-Drop [36]	60.96	$1.64 \times 10^{-4}$	$2.50 \times 10^{-3}$	90
High-Drop [36]	57.87	$1.87 \times 10^{-4}$	$2.50 \times 10^{-3}$	103
Critical Neighbor [28]	14.02	$1.01 \times 10^{-4}$	$2.49 \times 10^{-3}$	97
Ours	<b>77.86</b>	<b><math>9.72 \times 10^{-5}</math></b>	$1.06 \times 10^{-2}$	<b>27</b>

(b) Point Addition

Table 2. Attack performance to PointNet on OBJ\_BG variant of ScanObjectNN.

Chamfer and Hausdorff distance from the adversarial examples to the input point cloud. We also observe that there is a tradeoff between perceptibility and the number of perturbed points, e.g., the Hausdorff distance is higher than that of the baselines to account for smaller number of points perturbed. Fig. 1 visualises the adversarial point clouds generated by our method from ModelNet40 dataset. As can be seen, compared with other baselines, our method less likely produces outliers. This is due to the use of constraints on the object perceptibility in our adversarial generation formula.

Experimental results also show that, point addition performs best among all adversarial generation strategies. In addition, although the success rate of point addition is generally lower than that of point perturbation, point addition requires fewer points and maintains better perceptibility.

To capture the performance trend, we further plot the success rate over different number of points manipulated in the perturbation. Fig. 3 illustrates the result. The graph shows that our method outperforms other methods significantly especially when a small set of points are perturbed.

#### 4.2.3 Real-world Data

We also evaluate our method on the entire real-world dataset, ScanObjectNN. Recall that ScanObjectNN has five variants corresponding to five challenges, e.g., “OBJ\_BG” includes objects with background, “PB\_T25” includes objects translated by 25%, post-fixes “R” and “S” denote rotated and scaled objects, respectively. Readers are referred to [25] for more details of ScanObjectNN dataset. We report the attack performance of our method to PointNet on

the entire ScanObjectNN dataset in Table 3. As shown in experimental results, our method maintains a success rate from 80% to 89% by using only 3% of total points. In addition, we observe that, compared with OBJ\_BG, other variants show higher success rates and lower Hausdorff distance. We show several adversarial examples generated by our method from two variants of ScanObjectNN in Fig. 2. In general, compared with OBJ\_BG, adversarial examples on PB\_T50\_RS are much harder to recognise. This shows the vulnerability of real-world data and also suggests the necessity to validate attack techniques on extreme situations with minimum attacks. Fig. 4 shows the performance trend of point perturbations on ScanObjectNN.

#### 4.2.4 Other Network Architectures

To demonstrate that our method is agnostic to the underlying network, we further evaluate our method on PointNet++ [20], an extension of PointNet to learn local features. PointNet++ achieves the state-of-the-art performance in point cloud object classification. Attack results to PointNet++ are reported in Table 4. Experimental results on both PointNet and PointNet++ confirm that existing point cloud networks become vulnerable even when a small number of points in point clouds are perturbed.

#### 4.2.5 Adversarial Defenses

Finally, we evaluate how our adversarial point clouds can be defended. In this experiment, we use two basic defense techniques [13]: outlier removal and salient point removal.

Variant	Success Rate	Chamfer Distance	Hausdorff Distance	# Points
OBJ_BG	84.37	$9.83 \times 10^{-5}$	$1.01 \times 10^{-2}$	28
PB_T25	89.73	$9.74 \times 10^{-5}$	$9.79 \times 10^{-3}$	31
PB_T25_R	89.97	$7.80 \times 10^{-5}$	$7.85 \times 10^{-3}$	28
PB_T50_R	88.90	$6.62 \times 10^{-5}$	$6.44 \times 10^{-3}$	30
PB_T50_RS	88.15	$6.73 \times 10^{-5}$	$6.80 \times 10^{-3}$	27

(a) Point Perturbation

Variant	Success Rate	Chamfer Distance	Hausdorff Distance	# Points
OBJ_BG	77.86	$9.72 \times 10^{-5}$	$1.06 \times 10^{-2}$	27
PB_T25	90.11	$9.42 \times 10^{-5}$	$1.04 \times 10^{-3}$	30
PB_T25_R	88.61	$7.61 \times 10^{-5}$	$8.41 \times 10^{-3}$	27
PB_T50_R	86.25	$6.47 \times 10^{-5}$	$6.73 \times 10^{-3}$	27
PB_T50_RS	82.83	$6.48 \times 10^{-5}$	$6.63 \times 10^{-3}$	31

(b) Point Addition

Table 3. Attack performance to PointNet on entire ScanObjectNN.

	Success Rate	Chamfer Distance	Hausdorff Distance	# Points
ModelNet40	73.92	$4.54 \times 10^{-4}$	$3.69 \times 10^{-2}$	33
OBJ_BG	90.44	$1.85 \times 10^{-4}$	$1.76 \times 10^{-2}$	32

(a) Point Perturbation

	Success Rate	Chamfer Distance	Hausdorff Distance	# Points
ModelNet40	52.94	$2.96 \times 10^{-4}$	$2.68 \times 10^{-2}$	31
OBJ_BG	75.61	$1.50 \times 10^{-4}$	$1.37 \times 10^{-2}$	30

(b) Point Addition

Table 4. Attack performance to PointNet++.

The outlier removal technique first estimates statistical outliers from the point set and removes points that have large standard deviations. The salient point removal operates by first estimating point saliency and then points from high to low saliency are removed in order. We show defense results in Table 4.2.5. In general, it is moderately easy to defend our adversarial point clouds using the above methods, with success rate up to 92% of all adversarial examples on ModelNet40. Despite that, we found that such defenses on real-world data in ScanObjectNN are less effective compared to that of CAD models in ModelNet40: the success rate is decreasing with harder variants in ScanObjectNN. Together with the fact that real-world data is also more vulnerable to attacks, this raises significant concerns in applying deep learning to 3D point clouds in practice.

## 5. Conclusion

In this work, we introduced a general formulation to generate adversarial examples of 3D point clouds via  $\ell_0$  optimisation. Our method supports point perturbation and point

addition in a unified framework. We showed that point cloud neural networks like PointNet and PointNet++ are vulnerable to attacks that perturb approximately 40/1,024 points, which is only 4% of the total number of points. This result poses significant challenges in developing countermeasures to defend against such attacks. We also demonstrated that point clouds acquired from the real-world data are even more vulnerable. More studies on the relation between synthetic and real-world data and how it influences adversarial examples would be highly recommended.

With increasingly more 3D data used in consumer devices, we envision that adversarial attacks and defenses for point clouds will become very diverse, making this topic worthy of future research. First, here we only investigated how to perturb the 3D coordinates of a point cloud. For real-world data acquired from depth sensors, colour information is also available and could serve as an additional channel for adversarial attacks. It would be useful to study how such information influences the vulnerability of 3D deep learning. Besides, it is important to investigate how to implement ad-

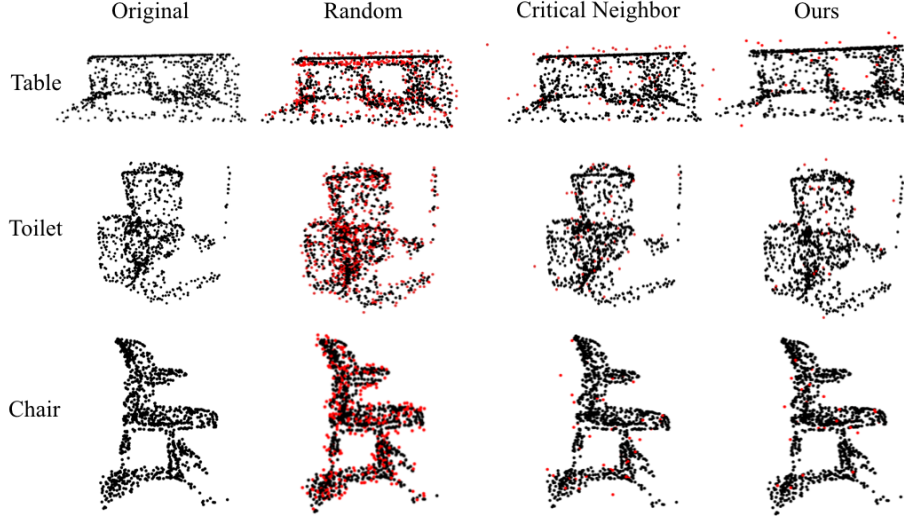


Figure 2. Adversarial examples generated by our method from ScanObjectNN dataset (on OBJ\_BG variant). Red points represent selected points.

Dataset	Outlier removal [13]	Salient point removal [13]
ModelNet40	92.60	94.51
OBJ_BG	91.55	95.10
PB_T25	87.67	92.02
PB_T25_R	86.91	91.02
PB_T50_R	84.55	90.48
PB_T50_RS	85.09	89.70

(a) Point Perturbation

Dataset	Outlier removal [13]	Salient point removal [13]
ModelNet40	93.97	95.23
OBJ_BG	90.12	94.61
PB_T25	87.38	92.68
PB_T25_R	87.20	92.20
PB_T50_R	86.41	90.59
PB_T50_RS	85.09	89.70

(b) Point Addition

Table 5. Defense performance.

versarial point clouds in the physical world. The results of this work show that such an implementation could be practical as only a few percentages of the input point cloud need to be modified.

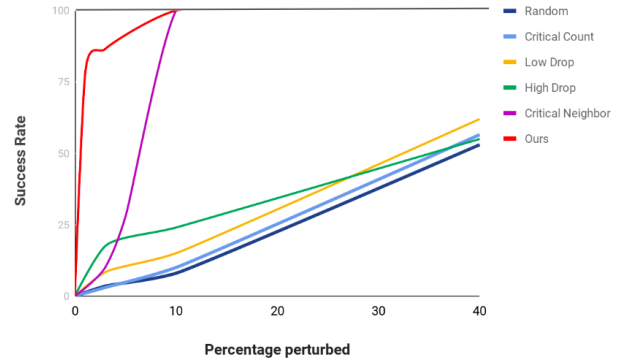


Figure 3. The performance trend of our adversarial attack on the ModelNet40 dataset. Our method is more effective than all other methods, requiring only  $\approx 4\%$  of all points to be perturbed to reach 80% success rate.

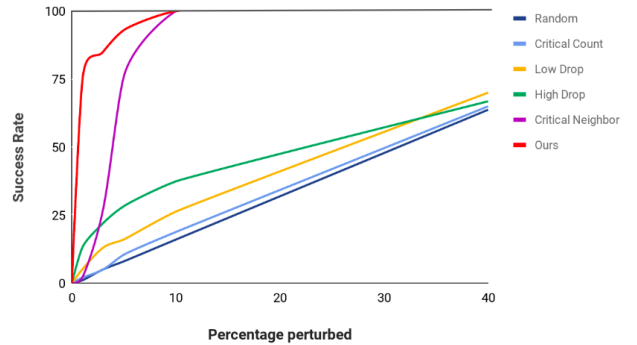


Figure 4. The performance trend of our adversarial attack on the OBJ\_BG variant of the ScanObjectNN dataset. Again, our method outperforms all remaining methods despite only a small percentage of perturbations is performed.



## References

- [1] Iro Armeni, Ozan Sener, Amir R Zamir, Helen Jiang, Ioannis Brilakis, Martin Fischer, and Silvio Savarese. 3d semantic parsing of large-scale indoor spaces. In *CVPR*, 2016. 1
- [2] Angel Chang, Angela Dai, Thomas Funkhouser, Maciej Halber, Matthias Niessner, Manolis Savva, Shuran Song, Andy Zeng, and Yinda Zhang. Matterport3d: Learning from rgb-d data in indoor environments. *International Conference on 3D Vision (3DV)*, 2017. 1
- [3] Angel X. Chang, Thomas A. Funkhouser, Leonidas J. Guibas, Pat Hanrahan, Qi-Xing Huang, Zimo Li, Silvio Savarese, Manolis Savva, Shuran Song, Hao Su, Jianxiong Xiao, Li Yi, and Fisher Yu. Shapenet: An information-rich 3d model repository. In *arXiv:1512.03012*, 2015. 1
- [4] Francesco Croce and Matthias Hein. Sparse and imperceivable adversarial attacks. In *The IEEE International Conference on Computer Vision (ICCV)*, 2019. 2
- [5] Angela Dai, Angel X Chang, Manolis Savva, Maciej Halber, Thomas Funkhouser, and Matthias Niessner. Scannet: Richly-annotated 3d reconstructions of indoor scenes. In *CVPR*, pages 5828–5839, 2017. 1
- [6] Ian Goodfellow, Jonathon Shlens, and Christian Szegedy. Explaining and harnessing adversarial examples. In *International Conference on Learning Representations*, 2015. 2, 3
- [7] Binh-Son Hua, Quang-Hieu Pham, Duc Thanh Nguyen, Minh-Khoi Tran, Lap-Fai Yu, and Sai-Kit Yeung. Scenenn: A scene meshes dataset with annotations. In *International Conference on 3D Vision*, 2016. 1
- [8] Binh-Son Hua, Minh-Khoi Tran, and Sai-Kit Yeung. Pointwise convolutional neural network. In *CVPR*, 2018. 2
- [9] Qiangui Huang, Weiye Wang, and Ulrich Neumann. Recurrent slice networks for 3d segmentation on point clouds. In *CVPR*, 2018. 2
- [10] Diederick P Kingma and Jimmy Ba. Adam: A method for stochastic optimization. In *International Conference on Learning Representations (ICLR)*, 2015. 11
- [11] Yangyan Li, Rui Bu, Mingchao Sun, and Baoquan Chen. Pointcnn: Convolution on x-transformed points. *Advances in Neural Information Processing Systems*, 2018. 2
- [12] Daniel Liu, Ronald Yu, and Hao Su. Adversarial point perturbations on 3d objects. *arXiv preprint arXiv:1908.06062*, 2019. 1, 2
- [13] Daniel Liu, Ronald Yu, and Hao Su. Extending adversarial attacks and defenses to deep 3d point cloud classifiers. In *The IEEE International Conference on Image Processing (ICIP)*, 2019. 1, 2, 3, 6, 8
- [14] Apostolos Modas, Seyed-Mohsen Moosavi-Dezfooli, and Pascal Frossard. Sparsefool: A few pixels make a big difference. In *The IEEE Conference on Computer Vision and Pattern Recognition (CVPR)*, 2019. 2
- [15] Nina Narodytska and Shiva Prasad Kasiviswanathan. Simple black-box adversarial perturbations for deep networks. *arXiv:1612.06299*, 2016. 2
- [16] David Wagner Nicholas Carlini. Towards evaluating the robustness of neural networks. In *IEEE Symposium on Security and Privacy (SP)*, 2017. 2
- [17] Nicolas Papernot, Patrick D. McDaniel, Somesh Jha, Matt Fredrikson, Z. Berkay Celik, and Ananthram Swami. The limitations of deep learning in adversarial settings. In *IEEE European Symposium on Security and Privacy, EuroS&P 2016, Saarbrücken, Germany, March 21-24, 2016*, pages 372–387. IEEE, 2016. 2
- [18] Adrien Poulenard, Marie-Julie Rakotosaona, Yann Ponty, and Maks Ovsjanikov. Effective rotation-invariant point cnn with spherical harmonics kernels. *International Conference on 3D Vision (3DV)*, 2019. 2
- [19] Charles R Qi, Hao Su, Kaichun Mo, and Leonidas J Guibas. Pointnet: Deep learning on point sets for 3d classification and segmentation. In *CVPR*, 2017. 2, 3, 4, 12
- [20] Charles Ruizhongtai Qi, Li Yi, Hao Su, and Leonidas J Guibas. Pointnet++: Deep hierarchical feature learning on point sets in a metric space. In *Advances in Neural Information Processing Systems*, pages 5105–5114, 2017. 2, 6, 12
- [21] Yongming Rao, Jiwen Lu, and Jie Zhou. Spherical fractal convolutional neural networks for point cloud recognition. In *Computer Vision and Pattern Recognition (CVPR)*, 2019. 2
- [22] Lukas Schott, Jonas Rauber, Matthias Bethge, and Wieland Brendel. Towards the first adversarially robust neural network model on MNIST. In *7th International Conference on Learning Representations, ICLR 2019, New Orleans, LA, USA, May 6-9, 2019*. OpenReview.net, 2019. 2
- [23] Yiru Shen, Chen Feng, Yaoqing Yang, and Dong Tian. Mining point cloud local structures by kernel correlation and graph pooling. In *CVPR*, volume 4, 2018. 2
- [24] Jiawei Su, Danilo Vasconcellos Vargas, and Kouichi Sakurai. One pixel attack for fooling deep neural networks. *IEEE Trans. Evolutionary Computation*, 23(5):828–841, 2019. 2
- [25] Mikaela Angelina Uy, Quang-Hieu Pham, Binh-Son Hua, Duc Thanh Nguyen, and Sai-Kit Yeung. Revisiting point cloud classification: A new benchmark dataset and classification model on real-world data. In *International Conference on Computer Vision (ICCV)*, 2019. 1, 2, 4, 6
- [26] Yue Wang, Yongbin Sun, Ziwei Liu, Sanjay E. Sarma, Michael M. Bronstein, and Justin M. Solomon. Dynamic graph cnn for learning on point clouds. *ACM Transactions on Graphics*, 2019. 2
- [27] Yuxin Wen, Jiehong Lin, Ke Chen, and Kui Jia. Geometry-aware generation of adversarial and cooperative point clouds. In *arXiv:1902.10899*, 2019. 1, 2
- [28] Matthew Wicker and Marta Kwiatkowska. Robustness of 3d deep learning in an adversarial setting. In *The IEEE Conference on Computer Vision and Pattern Recognition (CVPR)*, 2019. 2, 3, 4, 5, 6
- [29] Zhirong Wu, Shuran Song, Aditya Khosla, Fisher Yu, Linguang Zhang, Xiaoou Tang, and Jianxiong Xiao. 3d shapenets: A deep representation for volumetric shapes. In *The IEEE Conference on Computer Vision and Pattern Recognition (CVPR)*, 2015. 1, 2, 4
- [30] Chong Xiang, Charles R. Qi, and Bo Li. Generating 3d adversarial point clouds. In *IEEE Conference on Computer Vision and Pattern Recognition (CVPR)*, pages 9136–9144, 2019. 1, 2, 3, 4, 12

- [31] Jiancheng Yang, Qiang Zhang, Rongyao Fang, Bingbing Ni, Jinxian Liu, and Qi Tian. Adversarial attack and defense on point sets. In *arXiv:1902.10899*, 2019. 1, 2
- [32] Yang You, Yujing Lou, Qi Liu, Yu-Wing Tai, Lizhuang Ma, Cewu Lu, and Weiming Wang. Pointwise rotation-invariant network with adaptive sampling and 3d spherical voxel convolution. In *AAAI Conference on Artificial Intelligence*, 2020. 2
- [33] X. Yuan, P. He, Q. Zhu, and X. Li. Adversarial examples: Attacks and defenses for deep learning. *IEEE Transactions on Neural Networks and Learning Systems*, 30(9):2805–2824, 2019. 2
- [34] Zhiyuan Zhang, Binh-Son Hua, David W. Rosen, and Sai-Kit Yeung. Rotation invariant convolutions for 3d point clouds deep learning. In *International Conference on 3D Vision (3DV)*, pages 204–213, 2019. 2
- [35] Zhiyuan Zhang, Binh-Son Hua, and Sai-Kit Yeung. Shell-net: Efficient point cloud convolutional neural networks using concentric shells statistics. In *International Conference on Computer Vision (ICCV)*, pages 1607–1616, 2019. 2
- [36] Tianhang Zheng, Changyou Chen, Junsong Yuan, Bo Li, and Kui Ren. Pointcloud saliency maps. In *The IEEE International Conference on Computer Vision (ICCV)*, 2019. 2, 3, 4, 5, 6
- [37] Hang Zhou, Kejiang Chen, Weiming Zhang, Han Fang, Wenbo Zhou, and Nenghai Yu. Dup-net: Denoiser and up-sampler network for 3d adversarial point clouds defense. In *The IEEE International Conference on Computer Vision (ICCV)*, 2019. 2

# Supplementary Materials

## Abstract

In this supplementary document, we discuss our implementation details, which includes an extra relaxation to make our method easy to implement in Tensorflow. We then provide more quantitative and qualitative experiments on our adversarial attacks. We show that our optimization can easily converge and be insensitive to initialization values. We then provide additional visualizations to the performance trend of our method on the point addition case. Finally, we show an experimental transferability test in which adversarial examples generated by our method on PointNet is applied to PointNet++ and vice versa.

## A. Implementation Details

Recall that in the main paper (Equation 5), to generate the adversarial examples, we need to optimize the following cost function:

$$\min_{\mathbf{a}, E} f(P, \mathbf{a}, E) = \min_{\mathbf{a}, E} \{ \lambda_1 \|\mathbf{a}\|_1 + \lambda_2 D(P, P') + \lambda_3 h(P') \} \quad (10)$$

where the relation between the perturbed point cloud  $P'$  and the original point cloud  $P$  is

$$P' = \{ \mathbf{p}'_i = \mathbf{p}_i + a_i \mathbf{e}_i \mid \mathbf{p}_i \in P \} . \quad (11)$$

Note that here  $a_i \in \{0, 1\}$  is binary, and  $\mathbf{e}_i$  is continuous. Theoretically, it is necessary to use integer programming and linear programming to optimize this cost function. In practice, we use unconstrained optimization in Tensorflow to implement the optimization by relaxing  $a_i$  to be continuous. We only perform a clip to make  $a_i \in [0, 1]$ . Note that this is plausible given the L1-norm formulation in our case since most of values in vector  $\mathbf{a}$  becomes zero after the optimization. It is not necessary to binarize non-zero values of  $\mathbf{a}$  to  $\{0, 1\}$  either because eventually we only need the product of  $a_i \mathbf{e}_i$  to perturb the original point cloud. We found that such relaxation is plausible and our optimization converges in practice.

Consequently, the iterative updates for variable  $\mathbf{a}$  can be written as

$$a_i^{(n+1)} = a_i^{(n)} - \gamma \frac{\partial f}{\partial a_i} \quad (12)$$

where  $a_i^{(n)}$  is the solution at the  $n$ -th step and  $\gamma$  is calculated using Adam [10].

For point addition, we allow maximum 1024 points to be added. We found this way of implementation does not affect the performance as most elements of are zero. Below, we show an empirical test where continuous values of are rounded to binary or kept as is. As can be seen in Table 6, the difference is minor.

Rounding	Success Rate	# Points
No rounding	83.488372	25.693
With rounding	83.488372	26.939

(a) Point perturbation

Table 6. Rounding in point perturbation on OBJ\_BG

	Success Rate	# Points
Random	89.92	47
Critical Points	86.51	34

(a) Point perturbation

	Success Rate	# Points
Random	89.35	49
Critical Points	84.00	31

(b) Point addition

Table 7. Different initialization values of our optimization on ModelNet40.

Initialization	Success Rate	# Points
Random	90.0	41
Critical Points	84.37	28

(a) Point perturbation

Initialization	Success Rate	# Points
Random	89.53	41
Critical Points	77.86	27

(b) Point addition

Table 8. Different initialization values of our optimization on OBJ\_BG.

## B. Initialization

We test the various initialization methods for vector  $\mathbf{a}$  in Equation (10). For PointNet, we compare random and critical point initialization related to point perturbation and addition attack. Table 7 and 8 show that the initialization using critical points leads to results with good success rate and fewer point perturbations or additions. This result thus advocates the use of saliency map for initialization. Using random initialization works well, too but this technique almost doubles the number of perturbed points.

## C. Additional Plots

In addition to the performance trend of point perturbation shown in the main paper, here we further provide the trend for point addition attack on both datasets compare with the other baseline methods. The results are shown in

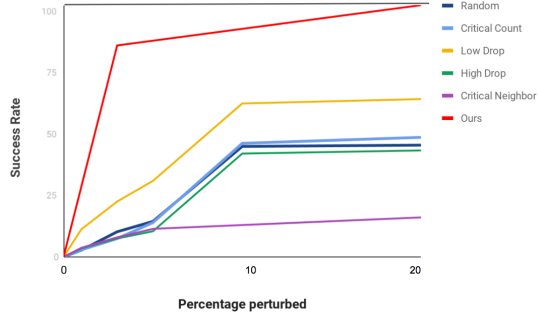


Figure 5. The performance trend of our point addition attack on the ModelNet40.

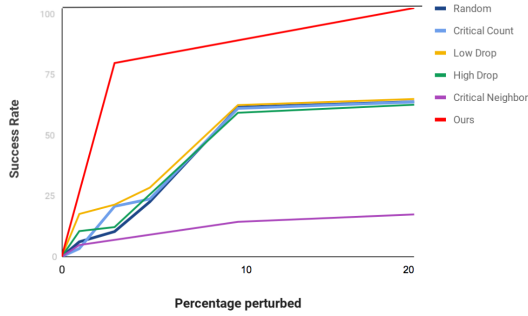


Figure 6. The performance trend of our point addition attack on the OBJ\_BG variant of the ScanObjectNN dataset.

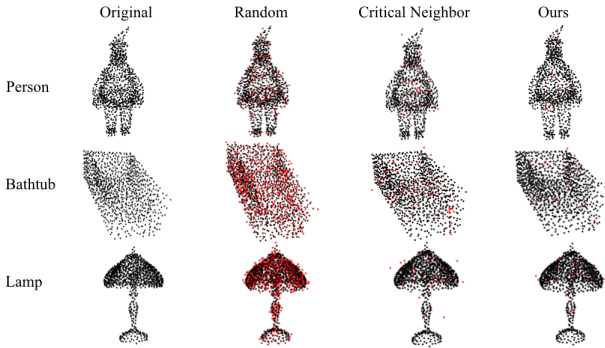


Figure 7. More adversarial examples from point perturbation on the ModelNet40.

Figure 5 and Figure 6.

## D. Additional Visualizations

In the section, we visualize more object categories for objects in ModelNet40 and ScanObjectNN’s OBJ\_BG and PB\_T50\_RS variant (Figure 7, 8, and 9). We also visualize the adversarial examples from point addition attack (Figure 10, 11, and 12).

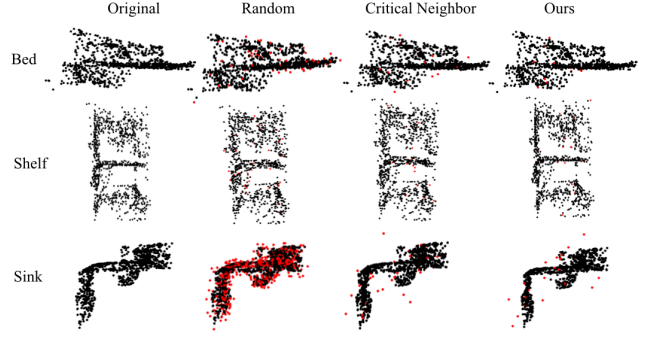


Figure 8. More adversarial examples from point perturbation on the OBJ\_BG variant of ScanObjectNN.

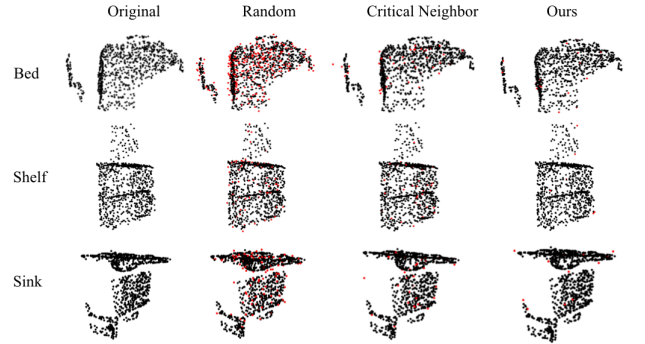


Figure 9. More adversarial examples from point perturbation on the PB\_T50\_RS variant of ScanObjectNN.

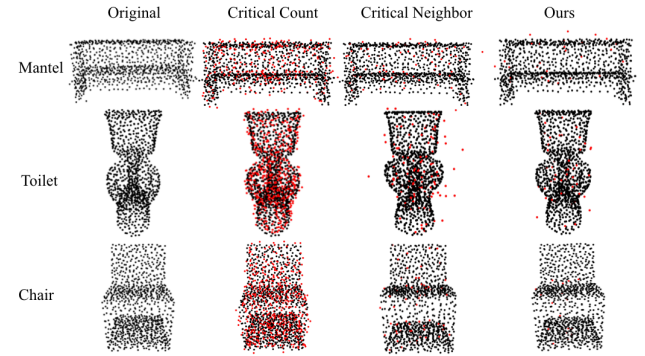


Figure 10. More adversarial examples from point addition on the ModelNet40.

## E. Transferability

We feed our adversarial point clouds made by PointNet [19] to the PointNet++ [20] as input. We find that both perturbation and addition attack is challenging to transfer and the results are shown Table 9. Such results are consistent to that by Xiang et al. [30]. In opposite, we also feed the adversarial examples on PointNet++ to PointNet. The transfer attack success about 20% with ModelNet40 and OBJ\_BG examples.

An interesting observation from the results is that the

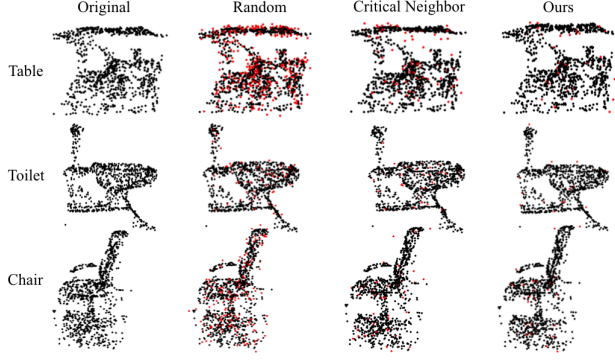


Figure 11. More adversarial examples from point addition on the OBJ\_BG variant of ScanObjectNN.

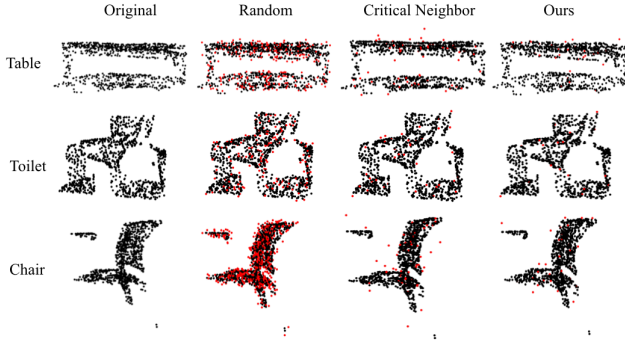


Figure 12. More adversarial examples from point addition on the PB\_T50\_RS variant of ScanObjectNN.

	Perturbation	Addition
ModelNet40	7.68	6.49
OBJ_BG	25.75	25.11
(a) PointNet to PointNet++		
	Perturbation	Addition
ModelNet40	25.66	22.34
OBJ_BG	19.55	20.94

(b) PointNet++ to PointNet

Table 9. We experiment with untargeted transfer attacks by generating the adversarial point clouds on PointNet and applying them to PointNet++ and vice versa. While the success rate is low, the results suggest that real-world data is more vulnerable to black box attacks.

real-world adversarial examples from ScanObjectNN are easier to transfer than synthetic examples in ModelNet40, which makes real-world data more vulnerable to black box attacks. This suggests the need to further make object classification for real-world data more accurate and robust.